HAL
open science

Error distribution in randomly perturbed orbits

Sandro Vaienti, Giorgio Turchetti, Francesco Zanlungo, Philippe Marie

To cite this version:

Sandro Vaienti, Giorgio Turchetti, Francesco Zanlungo, Philippe Marie. Error distribution in randomly perturbed orbits. Chaos: An Interdisciplinary Journal of Nonlinear Science, 2009, 19, pp.043118 (2009). 10.1063/1.3267510 . hal-00476224

HAL Id: hal-00476224

https://hal.science/hal-00476224

Submitted on 24 Apr 2010

HAL is a multi-disciplinary open access archive for the deposit and dissemination of scientific research documents, whether they are published or not. The documents may come from teaching and research institutions in France or abroad, or from public or private research centers.

L'archive ouverte pluridisciplinaire **HAL**, est destinée au dépôt et à la diffusion de documents scientifiques de niveau recherche, publiés ou non, émanant des établissements d'enseignement et de recherche français ou étrangers, des laboratoires publics ou privés.

AQ: #1

Error distribution in randomly perturbed orbits

Ph. Marie,[1,a)] G. Turchetti,[2,b)] S. Vaienti,[1,3,c)] and F. Zanlungo[2,d)]
[1]*Centre de Physique Théorique, CNRS, UMR-6207, Universités d'Aix-Marseille I, II, Provence-Alpes-Côte-d'Azur 13284, France and Université du Sud, Toulon-Var, Toulon 83130, France*
[2]*Department of Physics and Centro Galvani, University of Bologna, Bologna 40126, Italy*
[3]*Fédération de Recherche des Unités de Mathématiques de Marseille (FRUMAM), CPT, Luminy Case 907, F-13288 Marseille Cedex 9, France*

(Received 18 May 2009; accepted 3 November 2009; published online xx xx xxxx)

Given an observable f defined on the phase space of some dynamical system generated by the map T, we consider the error between the value of the function $f(T^n x_0)$ computed at time n along the orbit with initial condition x_0, and the value $f(T_\omega^n x_0)$ of the same observable computed by replacing the map T^n with the composition of maps $T_{\omega_n} \circ \cdots \circ T_{\omega_1}$, where each T_ω is chosen randomly, by varying ω, in a neighborhood of size ε of T. We show that the random variable $\Delta_n^\varepsilon \equiv f(T^n x_0) - f(T_{\boldsymbol{\omega}}^n x_0)$, depending on the initial condition x_0 and on the choice of the realization $\boldsymbol{\omega}$, will converge in distribution when $n \to \infty$ to what we call the *asymptotic error*. We study in detail the density of the distribution function of the asymptotic error for a wide class of dynamical systems perturbed with additive noise: for a few of them we give rigorous results, for the others we provide a numerical investigation. Our study is intended as a model for the effects of numerical noise due to roundoff on dynamical systems. © *2009 American Institute of Physics*. [doi:10.1063/1.3267510]

In the present paper we study the effect of a random perturbation on the orbit of a discrete dynamical system. We analyze the statistics of global errors Δ_n^ε, i.e., of the algebraic difference at iteration n between the exact orbit and an orbit perturbed at each step with a random error of order ε, by providing exact results for two model maps, regular and chaotic, respectively, and stating a general theorem on their asymptotics. This analysis suggests the existence of a time scale depending on ε for the convergence to the asymptotic error distribution. The scale is basically $\log(1/\varepsilon)$ for chaotic maps and ε^{-2} for regular maps and it is related to the interplay of the noise with the exponential or linear divergence of nearby orbits. The present paper provides, on rigorous grounds, the framework suitable to perform a systematic analysis of the statistics of the global error due to roundoff. In a future work and by using the numerical tools developed here, we will compare the results of this paper with those obtained using pure roundoff noise to check if the same qualitative behavior (i.e., the same time scales for the convergence to the asymptotic error distribution) holds.

I. INTRODUCTION

The reliability of numerical computations for discrete dynamical systems, where the only source of errors is due to the representation of real numbers by finite strings and to roundoff in arithmetic operations, is a long standing question. The algorithms used to implement roundoff arithmetic are not universal but depend on the hardware. As a consequence a rigorous analysis of the propagation of errors due to roundoff in floating point computations is largely incomplete.[1] The relative error η defined by $x^* = x(1+\eta)$, where x^* is the floating point representation of the real number x, grows when an iterative procedure is applied and the numerical orbit $x_n^* = T_* x_{n-1}^*$ may diverge with respect to the true orbit $x_n = T x_{n-1}$, where T is the map acting on the space X and T_* is its floating point representation. We also stress that the numerical inverse of a map T_*^{-1}, computed by implementing the algorithm which defines the true inverse T^{-1}, is not exact. The distance $d(\cdot,\cdot)$ between the true orbit and the numerical one is in general not known; however if in a single iteration it remains bounded $d(x_{n+1}^*, T x_n^*) \equiv d(T_* x_n^*, T x_n^*) < \varepsilon$, then we say that the numerical orbit is an ε pseudo-orbit, and some theoretical results are available if the map is mixing.

The reversibility error after n iterations $d(x_*, T_*^{-n} \circ T_*^n x_*)$ has a growth rate comparable to $d(T^n x_*, T_*^n x_*)$. Even though arithmetic with roundoff is deterministic it is often assumed that the sequence of errors is random. If so, letting $T x_n^* - T_* x_n^* = \varepsilon \xi_n$, the pseudo-orbit x_n^* appears to be generated by a map $T_* x = T x + \varepsilon \xi$ randomly perturbed with an additive noise. To prove that for any given initial point x_* the sequence ξ_n is actually equivalent to the realization of a random process and to specify its properties is once more a hard theoretical task. Nevertheless it is possible to investigate numerically the statistics of the pseudorandom sequence ξ_n by evaluating T with a much higher accuracy with respect to T_* so that we may neglect the difference with the exact result, at least below a significant time scale. To carry out this program it is critical to have some analytical estimates to guide our numerical investigations. In particular we need to know how the statistics of global errors $\Delta_n = T_*^n x_* - T^n x$ changes, evolving from the initial distribution $\rho_0(x) = \delta(x)$ to the asymptotic distribution $\rho_\infty(x)$. This program differs radically from the search of

[a)]Electronic mail: pmarie@cpt.univ-mrs.fr.
[b)]Electronic mail: turchetti@bo.infn.it.
[c)]Electronic mail: vaienti@cpt.univ-mrs.fr.
[d)]Electronic mail: zanlungo@bo.infn.it.

 © 2009 American Institute of Physics

a true orbit, close to the pseudo-orbit, whose existence is assured by the shadowing lemma.[2–8]

In the present work we compare the true orbit $T^n x_0$ and an ε-pseudo-orbit $\{x_n'\}_{n\geq 0}$ starting from the same initial point x_0 and analyze the probability distribution function of the algebraic error $f(T^n x_0)-f(x_n')$, where f is a smooth observable over X. More specifically we consider the case in which the pseudo-orbit is a random perturbation of the true orbit and provide analytical results to validate the numerical computations. The statistical analysis of actual roundoff errors is postponed to a forthcoming paper.

We consider a class $\mathcal{M}$ of dynamical systems with strong mixing properties (see Sec. II for a rigorous definition) for which exact results are proved and integrable dynamical systems as well. The error induced by a random perturbation of the map T in the computation of a smooth observable f is defined by

$$\Delta_n^\varepsilon = f(T^n x) - f(T_{\boldsymbol{\omega}}^n x), \tag{1}$$

where $T_{\boldsymbol{\omega}}^n = T_{\omega_1}\circ\cdots\circ T_{\omega_n}$, $|\omega_i|\leq\varepsilon$. This random variable is taken with respect to the probability measure given by the direct product of the Lebesgue measure m over X and the measure $\theta_\varepsilon^{\mathbb{N}}$ (see Sec. II) over the space of the realizations $\boldsymbol{\omega}$. The characteristic function φ_n^ε of the random variable Δ_n^ε is simply related to the *random* classical fidelity, introduced in Ref. 9, which is suited to investigate the statistics of the asymptotic error since it converges pointwise to

$$\varphi_n^\varepsilon(u) \to \mathbb{E}_\mu(e^{ifu})\overline{\mathbb{E}_{\mu_\varepsilon}(e^{ifu})}, \tag{2}$$

where the expectation values are calculated with respect to the invariant measure μ of the map T and to the stationary measure μ_ε of the stochastic perturbation T_ε of the map T (the bar denotes complex conjugation, see details in Sec. II). We show that this convergence is exponential with a rate which is related to the rate of decay of correlations. The left-hand side of Eq. (2) is the characteristic function of a random variable which we interpret as the *asymptotic error* and denote with $\Delta_\infty^\varepsilon$. This is the main quantity investigated in this paper.

The asymptotic error can be computed not only for chaotic maps but also for regular maps such as rotations. For the Bernoulli maps of the torus qx mod 1 and for rotations, a complete analytical study, providing detailed information about the transient to the asymptotic distribution, is possible.

Since the asymptotic error is the same for these prototypes of regular and chaotic maps, the difference must be searched for the transient, which reflects the divergence rate of nearby unperturbed orbits. In particular the asymptotic error is reached superexponentially fast for the Bernoulli map and just exponentially fast for rotations; in the first case the transition is very sharp, whereas it is smooth in the second case. The time scales for the convergence to the asymptotic error distribution are $n\sim\log(1/\varepsilon)$ and $n=\varepsilon^{-2}$, respectively. We also investigate, mostly numerically, systems with "intermediate" ergodic properties, such as intermittent maps, the logistic map, the Hénon attractor, and the standard map.

The plan of the paper is the following. Section II is devoted to analytical results for the class $\mathcal{M}$. In Sec. III we present the analytical results on two prototypes of regular and chaotic maps and compare them with numerical computations. In Sec. IV we present the results of numerical computations for several systems, where analytical results are missing: in particular we consider fractal attractors and follow the evolution looking at observables with a Cantorian structure. For these systems also the density distribution function for the asymptotic error has a fractal shape. Our major achievements are summarized in Sec. V and technical details are explained in Appendices A–D.

II. ERROR STATISTICS

A. Random perturbations and fidelity

Let X be a compact Riemannian manifold equipped with the Lebesgue measure m and consider a Borel measurable map $T:X\to X$ admitting a physical measure μ (very often also called SRB measure from Sinai, Ruelle, and Bowen who introduced it), which is defined through the limit

$$\lim_{n\to\infty}\int \psi\circ T^n dm = \int \psi d\mu, \tag{3}$$

where ψ is any continuous function over X. We introduce the random perturbation of the preceding system and successively we consider the fidelity as an interesting quantity to characterize the annealed correlation integrals arising under the stochastic perturbation.

Let $(\omega_k)_{k\in\mathbb{N}}$ be a sequence of independent and identically distributed (iid) random variables with values in the vector space Ω_ε and with distribution θ_ε. To each $\omega\in\Omega_\varepsilon$ we associate a map T_ω with $T_0=T$ and define the iterated perturbed map as $T_{\omega_n}\circ\cdots\circ T_{\omega_1}\equiv T_{\boldsymbol{\omega}}^n$.

According to Ref. 9 we consider a class of maps $\mathcal{M}$ such that the following are taken into account.

(i) The iterated perturbed map admits an invariant stationary measure μ_ε defined by

$$\lim_{n\to\infty}\int_X\int_{\Omega_\varepsilon^{\mathbb{N}}} \psi(T_{\boldsymbol{\omega}}^n x)d\theta_\varepsilon^{\mathbb{N}}(\boldsymbol{\omega})dm(x) = \int \psi d\mu_\varepsilon. \tag{4}$$

The distribution θ_ε is chosen in such a way that μ_ϵ will be absolutely continuous with respect to m (see Sec. II B), and moreover $\int_X\psi d\mu_\varepsilon\to\int_X\psi d\mu$ when $\varepsilon\to 0$ (stochastic stability).

(ii) The correlation integral decays exponentially on the space of $\mathcal{C}^1$ observables, i.e.,

$$\left|\int_X \psi_1(T^n x)\psi_2(x)dm(x) - \int_X \psi_1 d\mu\int_X \psi_2 dm\right| \leq C\lambda^{-n}\|\psi_1\|_1\|\psi_2\|_2, \tag{5}$$

where $C>0$ and $\lambda>1$ are determined only by the map T and the two norms depend on the map and on the space of observables (Ref. 9).

(iii) An exponential decay for the annealed correlation integral is assumed still for $\mathcal{C}^1$ functions,

$$\left| \int_X \int_{\Omega_\varepsilon^{\mathbb{N}}} \psi_1(T_{\boldsymbol{\omega}}^n x)\psi_2(x) d\theta_\varepsilon^{\mathbb{N}}(\boldsymbol{\omega}) dm(x) - \int_X \psi_1 d\mu_\varepsilon \int_X \psi_2 dm \right| \leq C\lambda^{-n}\|\psi_1\|_1\|\psi_2\|_2, \tag{6}$$

where C, λ, and the norms 1 and 2 are the same as in Eq. (5).

We introduce the *classical fidelity* by means of the following integral (this definition was inspired by Ref. 10):

$$F_n^\varepsilon = \int_X \int_{\Omega_\varepsilon^{\mathbb{N}}} \psi_1(T_{\boldsymbol{\omega}}^n x)\psi_2(T^n x) d\theta_\varepsilon^{\mathbb{N}}(\boldsymbol{\omega}) dm(x), \tag{7}$$

where ψ_1 and ψ_2 are C^1 functions.

It is possible to prove the following theorem (Ref. 9).

Theorem 1: *For the class $\mathcal{M}$ there exists a constant $C_1 > 0$ for which*

$$\left| F_n^\varepsilon - \int_X \psi_1 d\mu_\varepsilon \int_X \psi_2 d\mu \right| \leq C_1 \varepsilon^{-\kappa}\lambda^{-n}(\|\psi_2\|_1\|\psi_1\|_{C^0} + \|\psi_1\|_1\|\psi_2\|_{C^0}), \tag{8}$$

where $\|\cdot\|_1$ is a suitable norm on the space of observables and $\|\cdot\|_{C^0}$ is the supremum norm on continuous functions.

B. Additive noise

In this article we restrict ourselves to a particular random perturbation, the additive noise, which satisfies the assumptions of Theorem 1 and is well defined whenever the space X is the d-dimensional torus $X=\mathbb{T}^d$. In this case we define the random maps as $T_\omega = Tx+\omega \bmod \mathbb{T}^d$, where $\omega \in \mathbb{T}^d$, and then take θ_ε absolutely continuous with respect to the Lebesgue measure $d\omega$ over $\mathbb{T}^d$ and with a bounded density h_ε with support contained in the square $[-\varepsilon,\varepsilon]^d$ and such that $\int d\theta_\varepsilon = \int h_\varepsilon(\omega)d\omega = 1$. Letting $H(\xi)$ be a non-negative bounded function with support on $[-1,1]^d \subset \mathbb{R}^d$ such that $\int H(\xi)d\xi = 1$, the function $h_\varepsilon(x)$ is defined by $h_\varepsilon(\omega) = \varepsilon^{-d}H(\omega/\varepsilon)$. The change in variable $\omega = \varepsilon\xi$ shows that the density $h_\varepsilon(\omega)$ of the measure $\theta_\varepsilon(\omega)$ has the required properties. For the maps of the torus $\mathbb{T}$ discussed in Sec. III we consider a sequence of iid random variables $(\xi_k)_{k\in\mathbb{N}}$ in $[-1,1] \subset \mathbb{R}$ and a function $H(\xi)$ equal to 1/2 for $|\xi| \leq 1$ and equal to 0 for $|\xi| > 1$, limit of a sequence of normalized functions with support in $\xi \in [-1,1]$. As a consequence after the change $\omega = \varepsilon\xi$ the fidelity we compute reads

$$F_n^\varepsilon = 2^{-d}\int_0^1 dx \int_{-1}^1 d\boldsymbol{\xi}\psi_1(T^n x)\psi_2(T_{\varepsilon\xi_n} \circ \cdots \circ T_{\varepsilon\xi_1} x). \tag{9}$$

When the phase space X is a subset $D \in \mathbb{R}^n$, we require that the image of D is strictly included in D and that it remains so when randomly perturbed. It is straightforward to check that the orbits generated by maps perturbed with additive noise are ε pseudo-orbits. The equivalence between pseudo-orbits and random orbits holds for a wider class of noises, see Ref. 11.

Remark 1: Reference 9 gives several examples of dynamical systems satisfying Theorem 1: Anosov diffeomorphisms, uniformly hyperbolic attractors, piecewise expanding maps of the interval, and uniformly hyperbolic maps with singularities. Theorem 1 could be generalized by considering two randomly iterated perturbed maps $T_{\boldsymbol{\omega}}^n$ and $T_{\boldsymbol{\omega}'}^n$ having stationary measures μ_ε and μ_ε'. Equation (8), *where we replace T^n with $T_{\boldsymbol{\omega}'}^n$ and μ with μ_ε', would still hold. This result allows us to compare a randomly perturbed map with another one having a smaller perturbation when the exact map is not available as it happens in numerical computations.*

C. Error distribution

We consider the dynamical system (X,T,μ), where μ is a physical measure, and the family of random transformations T_{ω_k} previously defined. Let $f: X \to \mathbb{R}$ be a $\mathcal{C}^1$ observable and $m \otimes \theta_\varepsilon^{\mathbb{N}}$ be the probability measure on the product space $X \times \Omega_\varepsilon^{\mathbb{N}}$. The basic quantity investigated in this paper is the *algebraic error*

$$\Delta_n^\varepsilon = f(T^n x) - f(T_{\boldsymbol{\omega}}^n x)$$

given by the difference of two stochastic processes, for which we now state the following result that we use to investigate asymptotic distributions of errors.

Theorem 2: *Suppose the map $T \in \mathcal{M}$; then when n goes to $+\infty$, the random process Δ_n^ε, whose characteristic function is $\varphi_n^\varepsilon(u)$, converges in distribution to a random variable $\Delta_\infty^\varepsilon$ whose characteristic function is given by*

$$\varphi_\infty^\varepsilon(u) = \lim_{n\to\infty} \varphi_n^\varepsilon(u) = \int_X e^{iuf} d\mu \int_X e^{-iuf} d\mu_\varepsilon. \tag{10}$$

Proof: Indeed writing the characteristic function of the variable Δ_n^ε as $\varphi_n^\varepsilon(u)$ and using Fubini theorem, we have

$$\varphi_n^\varepsilon(u) \equiv \int_{X\times\Omega_\varepsilon^{\mathbb{N}}} e^{iu\Delta_n^\varepsilon(x,\boldsymbol{\omega})} dm(x) d\theta_\varepsilon^{\mathbb{N}}(\boldsymbol{\omega}) = \int_X \int_{\Omega_\varepsilon^{\mathbb{N}}} e^{iu[f(T^n x) - f(T_{\boldsymbol{\omega}}^n x)]} d\theta_\varepsilon^{\mathbb{N}}(\boldsymbol{\omega}) dm(x).$$

By Theorem 1 and by choosing $\psi_1(x) = e^{iuf(x)}$, $\psi_2(x) = e^{-iuf(x)}$ we immediately get the equality (10). Let us now denote with Φ_n^ε the distribution function of the variable Δ_n^ε; if we can prove that $\varphi_\infty^\varepsilon$ is continuous at $u=0$, then by Theorem 3, p. 266 in Ref. 12, we can conclude that $\varphi_\infty^\varepsilon$ is the characteristic function of some distribution function Φ_∞^ε and Φ_n^ε converges *completely* to Φ_∞^ε. In this case we will say that the random variables Δ_n^ε converge in *distribution* or *law* to a random variable, which we denote with $\Delta_\infty^\varepsilon$ and which has Φ_∞^ε as distribution function.

Since $|e^{\pm iuf}| \leq 1$ and μ and μ_ε are probability measures, by the dominated convergence theorem we immediately have that $\lim_{u\to 0} \varphi_\infty^\varepsilon(u) = 1 = \varphi_\infty^\varepsilon(0)$, which proves that $\varphi_\infty^\varepsilon$ is continuous at 0.

We are not really interested in the random variable $\Delta_\infty^\varepsilon$, but rather in its distribution function Φ_∞^ε. Whenever $\int_{-\infty}^{\infty} |\varphi_\infty^\varepsilon(u)| du < \infty$, the Lévy inversion formula asserts that the

distribution function Φ_∞^ε is absolutely continuous with a bounded continuous density ρ_∞^ε [probability density function (pdf)] given by

$$\rho_\infty^\varepsilon(t) = \frac{1}{2\pi}\int_{-\infty}^{\infty} e^{-iut}\varphi_\infty^\varepsilon(u)du. \tag{11}$$

We also note that the convergence to the asymptotic characteristic function is exponential but not uniform in the noise

$$|\varphi_n^\varepsilon(u) - \varphi_\infty^\varepsilon(u)| = \mathcal{O}(\varepsilon^{-\kappa}\lambda^{-n}). \tag{12}$$

This point is further investigated in Secs. III and IV and in Appendix D.

Remark 2: Since our random variable Δ_n^ε is bounded on X, all its moments are uniformly integrable and the moments of $\Delta_\infty^\varepsilon$ are given by the limit, for $n\to\infty$, of the corresponding moments of Δ_n^ε. In particular, we have

$$\text{(i)}\quad \mathbb{E}_{m\otimes\theta_\varepsilon^{\mathbb{N}}}(\Delta_\infty^\varepsilon) = \mathbb{E}_\mu(f) - \mathbb{E}_{\mu_\varepsilon}(f),$$

$$\begin{aligned}\text{(ii)}\quad \mathbb{V}_{m\otimes\theta_\varepsilon^{\mathbb{N}}}(\Delta_\infty^\varepsilon) &= \mathbb{V}_\mu(f) + \mathbb{V}_{\mu_\varepsilon}(f)\\ &= \int f^2 d\mu - \left(\int f d\mu\right)^2\\ &\quad + \int f^2 d\mu_\varepsilon - \left(\int f d\mu_\varepsilon\right)^2,\end{aligned}$$

where $\mathbb{E}_\nu$ (respectively $\mathbb{V}_\nu$) denotes the expectation (respectively the variance) with respect to the measure ν. Since we have assumed $\mu_\varepsilon\to\mu$ (stochastic stability), the average of the asymptotic error vanishes when $\varepsilon\to 0$, whereas its variance remains finite. This is a memory phenomenon because even if the noise vanishes after the system has evolved its effect persists. This is another consequence of the stochastic instability of the classical fidelity pointed out in Ref. 9. Additional considerations may be found in Appendix A, *where we compare our results with a recent related work by Sauer.*

III. ANALYTICAL RESULTS ON PROTOTYPE MAPS

A. Chaotic maps and rotations on the circle

As an easy illustration of the theorem 2 we consider the map T defined on one-dimensional (1D) torus $X=\mathbb{T}^1$ by $Tx = qx \bmod 1$, where $q\geq 2$ is a positive integer. We perturb it with additive noise producing the random transformations $T_{\varepsilon\xi}(x)=qx+\varepsilon\xi \bmod 1$, where $\varepsilon>0$ is the noise intensity and ξ is a random variable uniformly distributed over $[-1,1]$. By inspection of formula (4), it is easy to check that the noise just introduced has a stationary measure which coincides with the Lebesgue measure on $\mathbb{T}^1$. The map T clearly belongs to $\mathcal{M}$ and theorem 2 holds for smooth observables. We shall rather consider the observable *identity* $f(x)=x$ which is discontinuous on the torus. A direct proof of convergence will be given by using Fourier series, and we show in Sec. III B that the characteristic function of the asymptotic error is $\varphi_\infty^\varepsilon(u)=2u^{-2}(1-\cos u)$ [in agreement with Eq. (2)]. The asymptotic error is the triangular function on $[-1,1]$, namely, $\rho_\infty^\varepsilon(t)=(1-|t|)\mathbb{1}_{[-1,1]}$.

We apply the same Fourier analysis to regular maps, such as the translations on the torus $Tx=x+\chi \bmod 1$, which correspond to rotations of angle $2\pi\chi$ on the circle $\mathcal{C}^1$, and we perturb it with additive noise [we stress that for such maps our theorem 2 does not apply]. The random map iterated n times reads

$$T_{\varepsilon\xi}^n \equiv x + n\chi + \varepsilon(\xi_1+\xi_2+\cdots+\xi_n) \bmod 1, \tag{13}$$

where the $(\xi_l)_{l\geq 1}$ are iid random variables with common uniform distribution over $[-1,1]$. The Lebesgue measure on $\mathbb{T}^1$ is the unique stationary measure for the process. Let us consider the fidelity [Eq. (9)] F_n^ε for the function $\psi=\psi_1=\psi_2^*$ with Fourier coefficients $(\psi_k)_{k\in\mathbb{Z}}$. The function ψ is taken piecewise C^1 (at least) with a finite number of discontinuity points. Simple calculations give (see Appendix B)

$$F_n^\varepsilon = |\psi_0|^2 + \sum_{k\neq 0}|\psi_k|^2 S^n(k\varepsilon), \quad S(x) = \frac{\sin(2\pi x)}{2\pi x}. \tag{14}$$

The function S can be bounded by

$$|S(x)| \leq \begin{cases} e^{-\ln(2\pi)x^2} & \text{if } |x|<1\\ \dfrac{1}{2\pi|x|} & \text{if } |x|\geq 1.\end{cases} \tag{15}$$

Using this bound in Eq. (14) and since the Fourier coefficients are at least bounded by $|\psi_k|\leq C|k|^{-1}$, where C is a constant depending on the observable ψ, we get, after a few manipulations (see Appendix B for details),

$$|F_n^\varepsilon - |\psi_0|^2| \leq C^2((2-\varepsilon)e^{-\varepsilon^2 n(\ln(2\pi))} + 2\varepsilon(2\pi)^{-n}). \tag{16}$$

This result applies also to $\varphi_n^\varepsilon(u)$, which is the fidelity computed using $\psi=e^{iuf(x)}$.

B. Transients for the maps on the torus

Since Eq. (16) converges to zero and by taking $f(x)=x$, the asymptotic distribution of errors $\Delta_\infty^\varepsilon$ for rotations is again the triangular distribution, as in the case of $qx \bmod 1$ with $q\geq 2$. Therefore a chaotic and a very regular map (which *is* the identity for $\chi=0$) share the same distribution for the error between the true orbit and its random perturbation with the same initial condition. This is not surprising if one realizes that what we are doing for the observable identity $f(x)=x$ is just to compute the distribution of the difference of two points selected randomly, and independently one from the other, on the circle with uniform distribution: the distribution of the difference is just the triangular law. The previous required statistical assumptions are guaranteed by the Bernoulli property of the map $qx \bmod 1$ and by the independence and the common uniform distribution of the kicks ξ_l for rotations.

The very different ergodic properties of the two systems are reflected, however, in the rate of convergence to the limiting distribution. Equation (12) suggests an exponential decay for $\mathcal{M}$ maps [for $qx \bmod 1$ the exponent is $\kappa=1$ (Ref. 9)], but we can considerably improve the latter estimate using Fourier series and prove that the convergence for $qx \bmod 1$ is indeed superexponential. We first observe that

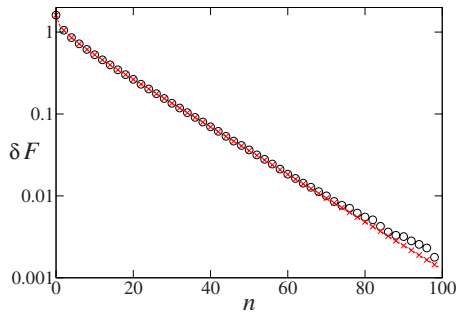

FIG. 1. (Color online) Comparison between the analytical result, Eq. (14), and Monte Carlo integrals for the decay of fidelity [Eq. (24)] in rotations, $\varepsilon=0.1$ (analytical result: red dashed line and crosses; Monte Carlo: circles). We used $N=10^7$ integration points in the Monte Carlo method. The test functions $\psi_1=\psi_2^*$ were defined in Fourier space as $\psi_k=k^{-1}$ truncated at $k=30$.

$$F_n^\varepsilon = |\psi_0|^2 + \sum_{k\neq 0} |\psi_k|^2 S_{n,q}(k\varepsilon), \tag{17}$$

where we have defined

$$S_{n,q}(x) = \prod_{k=0}^{k=n-1} S(q^k x) \tag{18}$$

(the proof of this equation is given in Appendix B). A bound for Eq. (17) can be found as

$$|F_n^\varepsilon - |\psi_0|^2| \leq \begin{cases} Ae^{-\alpha q^{2(n-n_*)}} & \text{if } n < n_* \\ Ae^{-\alpha} q^{-(n-n_*)^2/2} & \text{if } n \geq n_*, \end{cases} \tag{19}$$

where

$$\varepsilon q^{n_*} = 1 \quad \text{or} \quad n_* = -\log_q \varepsilon. \tag{20}$$

This formula shows a sharp transition in the decay whenever $n \sim \ln \varepsilon^{-1}/\ln q = n_*$ and the decay becomes superexponential. Instead, for rotations, such a transition point does not exist and the decay is smooth, see Figs. 1 and 2. The difference between these two regimes becomes also apparent when we compute ρ_n^ε, the distribution function of Δ_n^ε, for the identity observable, which is given by the inverse Fourier transform of the following characteristic functions that we obtain after evaluating the Fourier coefficients

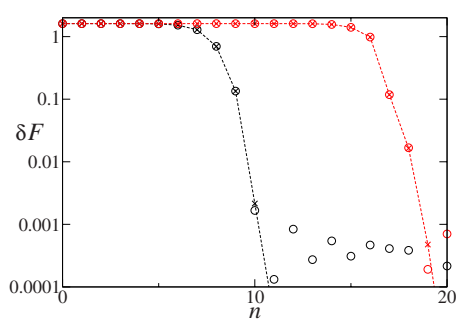

FIG. 2. (Color online) Comparison between the analytical result, Eq. (17), and Monte Carlo integral for the decay of fidelity [Eq. (24)] in $3x$ mod 1. $\varepsilon=10^{-4}$ in black and $\varepsilon=10^{-8}$ in red (gray in black and white) (analytical result: dashed line and crosses; Monte Carlo: circles). We used $N=10^7$ integration points in the Monte Carlo method. The test functions $\psi_1=\psi_2^*$ were defined in Fourier space as $\psi_k=k^{-1}$ truncated at $n=30$.

$$\psi_k = e^{i(u/2-\pi k)} \frac{\sin(u/2-\pi k)}{u/2-\pi k}$$

of the function $\psi(x)$ defined on the torus so that $\psi(x)=e^{iux}$ for $0 \leq x < 1$, namely,

$$\psi(x) = \begin{cases} e^{iu(x-[x])} & \text{if } x > 0 \\ e^{iu(1+x-[x])} & \text{if } x < 0, \end{cases} \tag{21}$$

where $[x]$ stands for the integer part of $x \in \mathbb{R}$ (this choice is equivalent to study e^{iux} defined on the torus). The result explicitly reads

$$\varphi_n^\varepsilon(u) = \frac{2}{u^2}(1-\cos u) + \sum_{k=1}^{\infty} S^n(k) \left[\frac{\sin^2(u/2-\pi k)}{(u/2-\pi k)^2} + \frac{\sin^2(u/2+\pi k)}{(u/2+\pi k)^2} \right] \tag{22}$$

for rotations and

$$\varphi_n^\varepsilon(u) = \frac{2}{u^2}(1-\cos u) + \sum_{k=1}^{\infty} S_{n,q}(k) \left[\frac{\sin^2(u/2-\pi k)}{(u/2-\pi k)^2} + \frac{\sin^2(u/2+\pi k)}{(u/2+\pi k)^2} \right] \tag{23}$$

for qx mod 1. See Appendix B for more details. The inverse Fourier transform of $2u^{-2}(1-\cos u)$ is the triangular distribution so that

$$\rho_\infty^\varepsilon(t) = (1-|t|)\mathbb{1}_{[-1,1]}.$$

The continuum limit of these processes is described in Appendix C.

C. Comparison to numerical results

We have compared the analytical results with the output of numerical computations based essentially on Eq. (9). The decay of fidelity [see also Eq. (8)] on $X=[0,1]$ is defined by

$$\delta F_n^\varepsilon = F_n^\varepsilon - 2^{-d}\left(\int_0^1 dx \psi_1(T^n(x))\right) \times \left(\int_0^1 dx \int_{-1}^1 d\boldsymbol{\xi} \psi_2(T_{\varepsilon\xi_n} \circ \cdots \circ T_{\varepsilon\xi_1} x)\right), \tag{24}$$

where F_n^ε is given by Eq. (9). The integrals are performed randomly choosing N vectors $(x,\boldsymbol{\xi})$ in $\mathbb{R}^{d(n+1)}$, i.e., using a Monte Carlo method whose accuracy is of order $N^{-1/2}$. For smooth test functions, integration methods with regularly distributed x points can improve the accuracy, but since for chaotic maps the smoothness of the integrand is rapidly lost and integration error estimates are difficult we systematically use a Monte Carlo on $(x,\boldsymbol{\xi})$ for which the error estimate $N^{-1/2}$ always holds. We show the comparison between the analytical and numerical results on the decay of fidelity for rotations (Fig. 1) and for the map $3x$ mod 1 (Fig. 2); while in Figs. 3–6 we compare the analytical results for ρ_n^ε [Fourier inversion of Eqs. (22) and (23)] with the corresponding numerical computations (i.e., with a Monte Carlo sampling of the error Δ_n^ε in which the probability function ρ_n^ε is approxi-

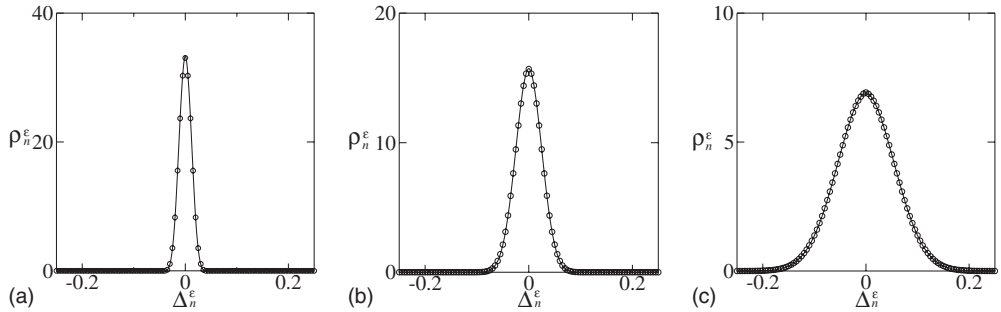

FIG. 3. Comparison between the analytical result for ρ_n^ε in rotations, Fourier transform of Eq. (22) (continuous line), and Monte Carlo sampling (circles), $\varepsilon=10^{-2}$. (a) $n=4$; (b) $n=19$; (c) $n=99$.

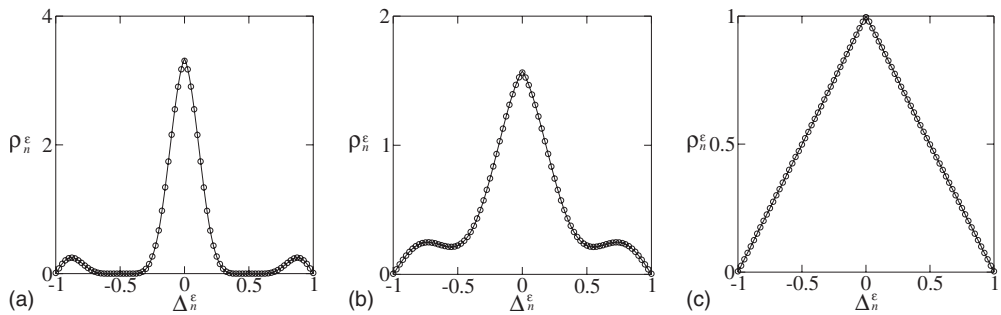

FIG. 4. Comparison between the analytical result for ρ_n^ε in rotations, Fourier transform of Eq. (22) (continuous line), and Monte Carlo sampling (circles), $\varepsilon=0.1$. (a) $n=4$; (b) $n=19$; (c) $n=99$. Compare the transition times with Fig. 1.

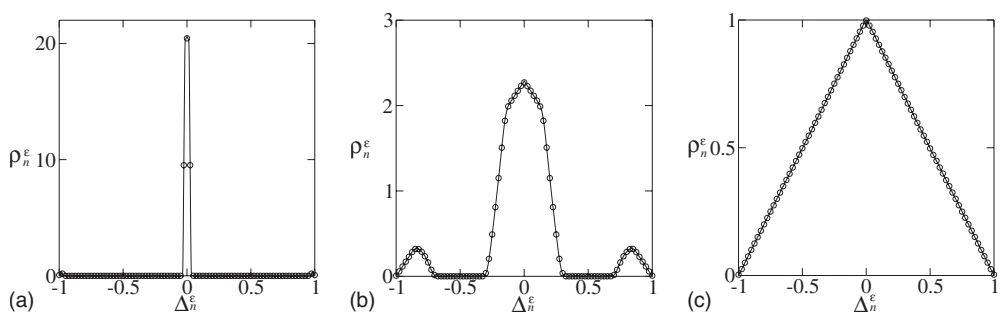

FIG. 5. Comparison between the analytical result for ρ_n^ε in $3x$ mod 1, Fourier transform of Eq. (23) (continuous line), and Monte Carlo sampling (circles), $\varepsilon=10^{-4}$. (a) $n=6$; (b) $n=8$; (c) $n=10$. Compare the transition times with Fig. 2.

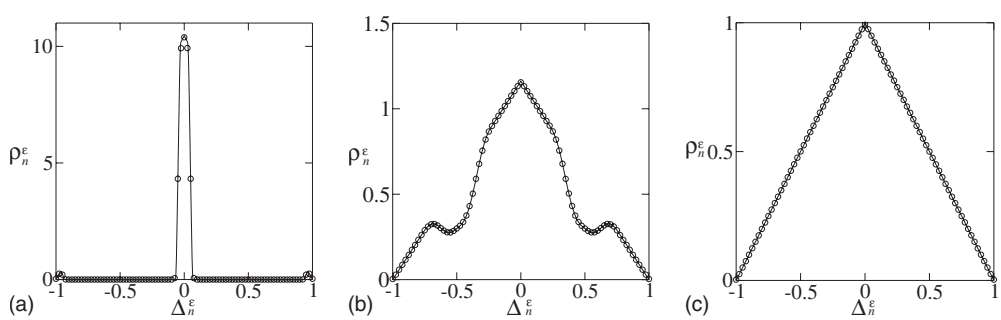

FIG. 6. Comparison between the analytical result for ρ_n^ε in $3x$ mod 1, Fourier transform of Eq. (23) (continuous line), and Monte Carlo sampling (circles), $\varepsilon=10^{-8}$. (a) $n=15$; (b) $n=17$; (c) $n=19$. Compare the transition times with Fig. 2.

mated by the probability of Δ_n^ε to be in an interval of length Δx).

These figures show clearly that while for rotations the transition from the initial condition $\rho_0^\varepsilon(x)=\delta(x)$ to the asymptotic (triangular) distribution is a gradual process, whose time scale is of order ε^{-2}, for the map $3x$ mod 1 we have a sharp transition that starts around $n_*=-\log_q \varepsilon$ [see Eq. (19)]. In the transition region the slope does not depend on ε but is related to the divergence of nearby orbits, namely, to the decay rate of correlations λ or the maximum Lyapunov exponent Λ (for several systems $\lambda=e^\Lambda$). According to Eq. (20) when ε varies from 10^{-4} to 10^{-8} the transition n_* varies by a factor of 2. For $n \ll n_*$ the error distribution function can be well approximated by a δ function, i.e., the perturbed system can be considered as equivalent to the unperturbed one.

In both regular and chaotic maps the asymptotic distribution is reached when δF_n approaches a value a few order of magnitude lower than the initial value. We remark that $\rho_n^\varepsilon(x)$ is the Fourier transform of $\varphi_n^\varepsilon(u)$, i.e., of the fidelity computed using $\psi_1=\psi_2^*=e^{iux}$. The comparison between the results in Figs. 1 and 2 and those in Figs. 3–6 suggests (as we have verified analyzing different test functions) that the decay of fidelity depends very weakly on the functions ψ_1, ψ_2, and thus that the analysis of a single, easily computable test function provides information about the evolution of $\rho_n^\varepsilon(x)$.

IV. NUMERICAL COMPUTATIONS

In this section we apply the theory developed above to various dynamical systems; for the majority of them it is not known whether all the conditions required to belong to the class $\mathcal{M}$ are satisfied. We compute numerically the distribution of the error ρ_n^ε for additive noise. The chosen observables are $f(x)=x$ for 1D maps and $f(\mathbf{x})=x$, $f(\mathbf{x})=y$ for two-dimensional (2D) maps. Whenever x parametrizes a linear subspace S of $\mathbb{R}$, the difference x_1-x_2 is the distance between x_1 and x_2 up to a sign. The integrals with respect to the physical measure and the stationary measure are performed by using their definition as weak limits of the Lebesgue measure. These limiting measures are no longer equal to the Lebesgue measure as in the examples in Sec. III. Two relevant classes of maps are considered. In the first one, which includes the maps with neutral fixed point(s) and the logistic map, the measures are absolutely continuous with respect to Lebesgue. In the second class, which includes the Hénon and the Baker's maps, the invariant measures are singular with respect to Lebesgue. For these maps the attractor has a fractal structure, which is locally described as the product of a smooth manifold with a Cantor set. When we deal with maps which are not hyperbolic and admit an absolutely continuous invariant measure with a density which is summable but not necessarily bounded (this is notably the case of the intermittent and quadratic maps), or when we have singular invariant measures as for the Hénon and the Baker's maps, we are not anymore sure that the characteristic function $\varphi_\infty^\varepsilon$ is Lebesgue integrable. We remind that this is a sufficient condition in order to apply the Lévy inversion formula (11). In Appendix D we explain what happens when we lose the summability of the characteristic function.

The numerical analysis consists of four steps.

- Decay of fidelity in a test function. On the basis of the results obtained for translations on the torus and for the map qx mod 1, we study the decay of fidelity [Eq. (24)] for the test function $\psi(x)=x$ (x observable) using a Monte Carlo method to compute the integrals. This analysis provides the values of n at which the transition from $\rho_0^\varepsilon=\delta(x)$ to the asymptotic regime ρ_∞^ε occurs.
- Computation of ρ_n^ε for significant values of n. Using a Monte Carlo sampling we perform the statistical analysis of Δ_n^ε, estimating its distribution ρ_n^ε, for the values of n suggested by the analysis in the first step.
- Asymptotic limit. The two previous steps allow us to identify a value $\bar{n}(\varepsilon)$ beyond which ρ_n^ε has reached its asymptotic value. We thus compute with high accuracy ρ_∞^ε as the average $\overline{\rho_{n'}^\varepsilon}$ over several values $n'>\bar{n}$.
- Check of the validity of Eq. (2). We compute $\varphi_\infty^\varepsilon$ using Eq. (2), and its Fourier transform, to check if it coincides with ρ_∞^ε that is computed with a Monte Carlo sampling, as predicted by Theorem 2.

Remark 3: In numerical computations, we cannot evaluate the error $\Delta_n^\varepsilon=f(T^n x)-f(T_{\boldsymbol{\omega}}^n x)$. In fact both T and T_ω are affected by the arithmetic roundoff, which in a single step introduces an error of order $\varepsilon_{\rm num}$. The orbit T^n is replaced by the perturbed orbit $T_{\boldsymbol{\omega}'}^n$, where ω_l' are now "random" variables in the space, say, $\Omega_{\varepsilon_{\rm num}}(0)$ around the unperturbed component 0. In the same way the random orbit $T_{\boldsymbol{\omega}}^n$ will be replaced by a new random orbit $T_{\boldsymbol{\omega}''}^n$, where the components ω_l'' are now random variables in the space $\Omega_{\varepsilon_{\rm num}}(\omega_l)$ around the component ω_l. Comparing $\Delta_n^{\varepsilon,\varepsilon_{\rm num}}=f(T_{\boldsymbol{\omega}'}^n x)-f(T_{\boldsymbol{\omega}''}^n x)$ with the analytical estimate for Δ_n^ε, or just letting $\varepsilon_{\rm num}\to 0$ by using arbitrary precision arithmetic, we can check that if $\varepsilon \gg \varepsilon_{\rm num}$, there is a time scale relevant for the study of Δ_n^ε, below which the additional error $\Delta_n^\varepsilon-\Delta_n^{\varepsilon,\varepsilon_{\rm num}}$ is negligible with respect to Δ_n^ε. Since the numerical roundoff error in double precision for a variable on the torus is of order $\varepsilon_{\rm num}\approx 10^{-16}$, we are going to use additive noise $\varepsilon>10^{-9}$. The choice $\varepsilon\approx 10^{-8}$, corresponding to single precision numerical roundoff, is of interest for future investigations on the statistics of roundoff errors in the iteration of maps. The convergence in distribution of the process $\Delta_n^{\varepsilon,\tilde{\varepsilon}}$ is guaranteed by the generalization of Theorem 1 provided in Remark 1. We observe that Sauer in Ref. 13 faced the same problem in developing a theory of true and perturbed orbits while checking the predictions of computer experiments. He wrote, "We computed the trajectory average in high precision (used to represent the "true" value) for a long trajectory and compared it with the trajectory computed with one-step random error of size ε."

A. Hénon map

The Hénon map is a 2D map defined by

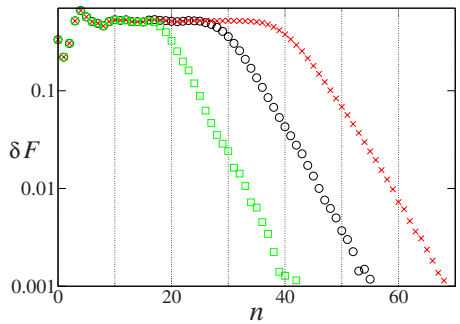

FIG. 7. (Color online) Decay of fidelity for the Hénon map, Monte Carlo integration with $N=10^7$. Green squares: $\varepsilon=10^{-4}$. Black circles: $\varepsilon=10^{-6}$. Red crosses: $\varepsilon=10^{-8}$.

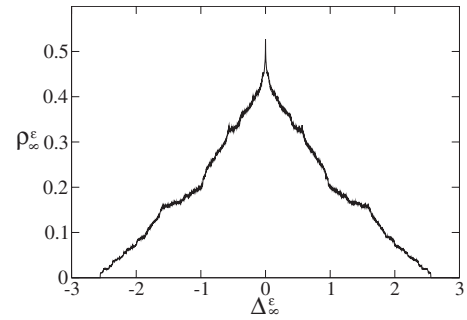

FIG. 9. ρ_∞^ε for the Hénon map with $\varepsilon=10^{-8}$, $f(\mathbf{x})=x$ given by the average of 10^6 samplings of ρ_n^ε, each one obtained using a Monte Carlo method with 10^3 starting points ($N=10^9$) and $\Delta x=10^{-3}$.

$$T\mathbf{x}=\begin{cases} x'=y+1-ax^2 \\ y'=bx. \end{cases} \tag{25}$$

We consider the canonical values $a=1.4$ and $b=0.3$, for which the map is known to be chaotic, at least numerically. We remind that Benedicks and Carleson[14] proved that there exists a set of positive Lebesgue measure S in the parameter space such that the Hénon map has a strange attractor whenever $(a,b)\in S$. The value of b is very small and the attractor lives in a small neighborhood of the x-axis. For those values of a and b, one can prove the existence of the physical measure and of a stationary measure under additive noise, which is supported in the basin of attraction and that converges to the physical measure in the zero noise limit.[15] It is still unknown whether such results could be extended to the "historical" values that we consider here.

The orbit starting at (x_0,y_0) will either approach the Hénon strange attractor or diverge to infinity. We study a connected subset D included in the basin of the attractor and define on it the perturbed map

$$T_{\varepsilon\boldsymbol{\xi}}\mathbf{x}=\begin{cases} x'=y+1-ax^2+\varepsilon\xi_x \\ y'=bx+\varepsilon\xi_y. \end{cases} \tag{26}$$

We have verified that using $D=(x,y)$ with $-1<x<1$ and $-1/2<y<1/4$ the set D is stable under small perturbations [i.e., the point (x_0,y_0) does not diverge to infinity under T_ε for small enough ε].

We studied the decay of fidelity [Eq. (24)] with observables x and y. After a transient that depends on the definition of the set D, the fidelity reaches a plateau, and then follows a decay phase (Fig. 7), whose rate does not depend on ε. The ε dependence is manifest in the outset of the decay (end of plateau). We name the value of n at which the decay phase starts n_* since its ε dependence is qualitatively compatible with Eq. (20). The height of the plateau, n_*, and the decay law are independent of the choice of D, as expected due to the ergodic properties of the map. The behavior of the y observable is almost the same as that of x. We successfully checked (Fig. 8) that the transition from $\rho_0^\varepsilon=\delta(x)$ to the asymptotic ρ_∞^ε starts with the outset of the decay phase of the fidelity (for example, around $n_*\approx 35$ in Fig. 7 for $\varepsilon=10^{-8}$). Below this time scale the error distribution function can be approximated by a δ function and thus the perturbed system can be considered as equivalent to the unperturbed one. We finally averaged ρ_n^ε over several $n>n_*$ in order to obtain ρ_∞^ε (Fig. 9) and checked, with good results, the validity of Eq. (2).

B. Baker's map

The Baker's map is defined by $T\mathbf{x}=\mathbf{x}'$, where

$$x'=\begin{cases} \gamma_a x \bmod 1 & \text{if } y<\alpha \\ \frac{1}{2}+\gamma_b x \bmod 1 & \text{if } y\geq\alpha, \end{cases}$$

$$y'=\begin{cases} \dfrac{y}{\alpha}\bmod 1 & \text{if } y<\alpha \\ \dfrac{y-\alpha}{1-\alpha}\bmod 1 & \text{if } y\geq\alpha, \end{cases}$$

while its perturbed version is

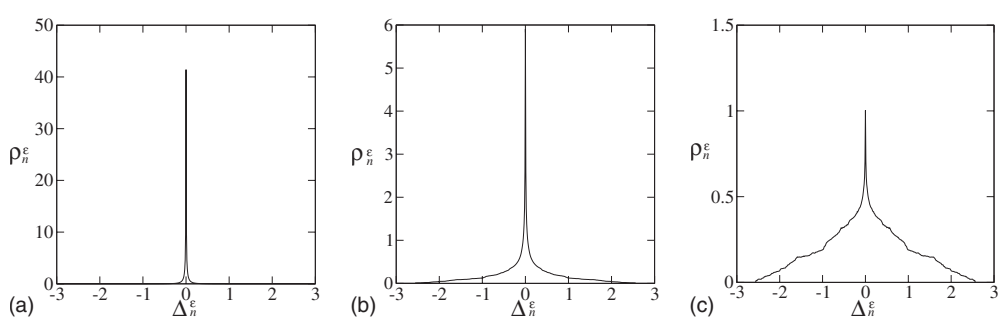

FIG. 8. ρ_n^ε for the Hénon map, $\varepsilon=10^{-8}$, $f(\mathbf{x})=x$. (a) $n=34$; (b) $n=44$; (c) $n=54$. Monte Carlo sampling using $N=10^8$ initial points and space discretization $\Delta x=10^{-2}$.

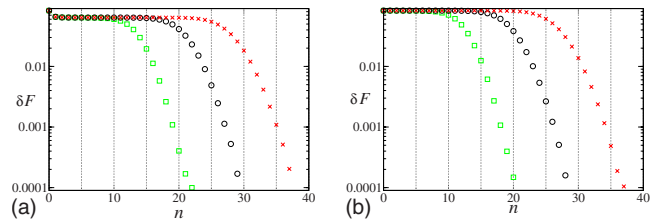

FIG. 10. (Color online) Decay of fidelity for the Baker's map, Monte Carlo integration with $N=10^7$. Green squares: $\varepsilon=10^{-4}$. Black circles: $\varepsilon=10^{-6}$. Red crosses: $\varepsilon=10^{-8}$. (a) x observable. (b) y observable.

$$T_{\varepsilon\xi}\mathbf{x} = (x' + \varepsilon\xi_x \bmod 1, y' + \varepsilon\xi_y \bmod 1).$$

Using $\gamma_a=\frac{1}{5}$, $\gamma_b=\frac{1}{4}$, and $\alpha=\frac{1}{3}$ we studied the decay of fidelity for the x and y observables (Fig. 10).

While the decay of fidelity for $\psi(\mathbf{x})=y$ shows a plateau and then a decay phase, for $\psi(\mathbf{x})=x$ the plateau is preceded by a decrease in the value of fidelity due to the convergence to the invariant measure. The difference between the first steps of fidelity for y and x is due to the different nature of the invariant distributions (uniform for y and a Cantor set for x); nevertheless the outset of fidelity decay (end of plateau) happens roughly at the same n_* for the two observables ($n_*\approx 20$ for $\varepsilon=10^{-8}$). Once again the ε dependence of n_* is in agreement with Eq. (20), and it is followed by an ε independent decay law. Also for this map the analysis of fidelity predicts quite well the outset of the transient from a delta function to the asymptotic distribution for the error distribution (not shown). While for $f(\mathbf{x})=y$, ρ_∞^ε is simply the triangular function, for the observable x we have a Cantor structure that can be better appreciated increasing the precision of the computation (Fig. 11). We also checked that Eq. (2) holds for this system. In order to understand the irregular shape of the pdf for the observable x, we modify the Baker's map in such a way to get the usual ternary Cantor set on the x-axis. This can be easily achieved by writing the modified Baker's map as

$$x' = \begin{cases} \dfrac{x}{3} & \text{if } y < \dfrac{1}{2} \\ \dfrac{1}{2} + \dfrac{x}{3} & \text{if } y \geq \dfrac{1}{2}, \end{cases} \tag{27}$$

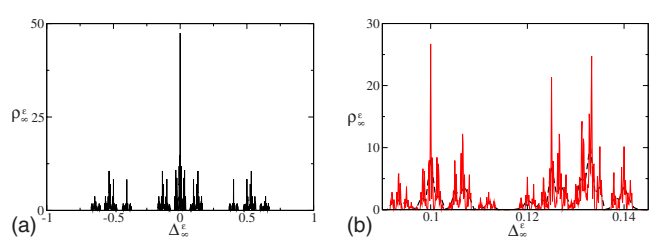

FIG. 11. (Color online) (a) ρ_∞^ε for the Baker's map, $\varepsilon=10^{-8}$, x observable. Monte Carlo sampling using $N=10^9$ and $\Delta x=10^{-3}$. (b) detail of ρ_∞^ε for the Baker's map, $\varepsilon=10^{-8}$, x observable. Black, dashed: Monte Carlo using $N=10^9$ and $\Delta x=10^{-3}$. Red, continuous: Monte Carlo using $N=10^{10}$ and $\Delta x=10^{-4}$.

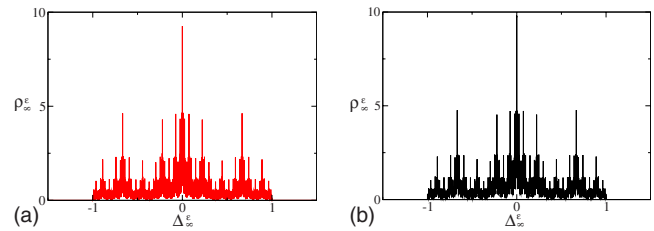

FIG. 12. (Color online) ρ_∞^ε for the modified Baker map (whose invariant measure corresponds to a ternary Cantor set) as obtained by Eq. (28) (a) and by Monte Carlo method (b).

$$y' = \begin{cases} 2y & \text{if } y < \frac{1}{2} \\ 2y - 1 & \text{if } y \geq \frac{1}{2}. \end{cases}$$

The physical SRB measure will be the direct product of an absolutely continuous measure along the y-axis and the singular Cantorian measure along the x-axis.[16] The latter is constructed as the weak limit of a sequence of measures which give equal weight 2^{-n} to the 2^n closed intervals of length 3^{-n} which contain the Cantor set for all n. The Fourier transform of this measure, say, μ_x, is known.[17] If we consider the observable x, the characteristic function of the asymptotic error will be $\int e^{ixu}d\mu_x\overline{\int e^{ixu}d\mu_\varepsilon}$. Let us suppose that the stationary measure is close to the SRB measure, which is the case since the Baker's transformation is uniformly hyperbolic, belongs to the class $\mathcal{M}$, and is stochastically stable. Therefore for small ε we could assume that the second integral in the preceding product is taken with respect to μ_x, and thus our characteristic function is $\varphi_\infty(u)=|\int e^{iux}d\mu_x|^2$. The latter can be computed: Zygmund[17] gives (see also Ref. 18 for a former study of this quantity)

$$\varphi_\infty(u) = \prod_{k=1}^{\infty} \cos^2[u3^{-k}]. \tag{28}$$

Zygmund also proved that $\varphi_\infty(u)$ is not summable and we recall that this is a sufficient condition in order to get the inversion formula (11). Despite this, we compute numerically the improper integral transform (11) and we get an excellent agreement with the numerical issues (Fig. 12). We outline that even if for any spatial discretization Δx we can numerically compute, obtaining the same result, the distribution function ρ_ε^n with three different methods [Monte Carlo sampling of errors falling in the interval $[x,x+\Delta x]$, inverse Fourier transform of Eq. (2), and inverse Fourier transform of Eq. (28)], we are not sure that the process converges in the $\Delta x\to 0$ limit, since the inverse Fourier transform could be ill defined (see Appendix D and the analogous discussion in Sec. IV C). Figure 11 shows clearly that at the numerically accessible Δx values the process still has not converged.

C. Intermittent map

The intermittent map on the torus is defined as

$$T_\alpha x = \begin{cases} x + 2^\alpha x^{\alpha+1} \bmod 1 & \text{if } 0 \leq x < \frac{1}{2} \\ x - 2^\alpha(1-x)^{\alpha+1} \bmod 1 & \text{if } \frac{1}{2} \leq x < 1 \end{cases} \tag{29}$$

with $0<\alpha<1$. It has been proved by several authors that the decay of correlations follows a power law as $n^{1-1/\alpha}$.[19–21] This

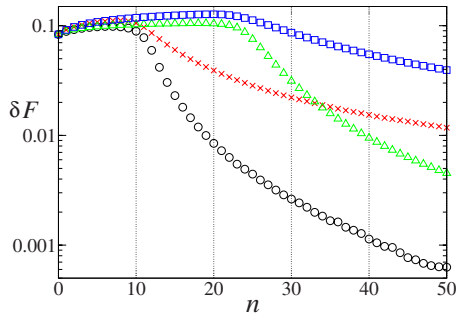

FIG. 13. (Color online) Decay of fidelity for the intermittent map, Monte Carlo integration with $N=10^7$. Black circles: $\varepsilon=10^{-4}$, $\alpha=0.5$. Red crosses: $\varepsilon=10^{-4}$, $\alpha=0.99$. Green triangles: $\varepsilon=10^{-8}$, $\alpha=0.5$. Blue squares: $\varepsilon=10^{-8}$, $\alpha=0.99$.

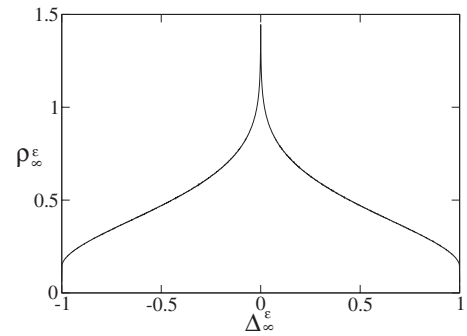

FIG. 14. ρ_∞^ε for the intermittent map, $\alpha=0.5$, $\varepsilon=10^{-8}$. Monte Carlo sampling using $N=10^9$ and $\Delta x=10^{-3}$.

rate is optimal in the sense that it gives also a lower bound for a large class of observables vanishing in a neighborhood of the neutral fixed point.[22,23] The density h of the absolutely continuous invariant measure has a singularity in the neighborhood of zero of the type $x^{-\alpha}$. The density h_ε of the stationary measure verifies the $\mathcal{L}_m^1$ estimate: $\|h-h_\varepsilon\|_{\mathcal{L}_m^1}\sim\varepsilon^{1-\alpha}$.[24] It is interesting to remark that the problem of the stochastic stability for this map is not fully understood. The papers[25,26] prove the weak convergence of the absolutely continuous stationary measure (under the additive noise) to a convex combination of the absolutely continuous invariant measure and of the Dirac mass at the neutral fixed point. The presence of this atomic measure in the weak limit is questionable; it prevents also any kind of strong convergence (in the $\mathcal{L}_m^1$ sense).

Our Monte Carlo integrations for the decay of correlations are compatible with the analytically predicted power law, even if an exact computation of the exponent of the power law is not feasible to a numerical analysis since the convergence to the predicted law is slow in n. The decay of fidelity for this map shows a growing phase (that depends on α and is due to the convergence to the asymptotic measure), an α independent outset of decay $n_*(\varepsilon)$ (end of "plateau") whose ε dependence is in qualitative agreement with Eq. (20), followed by an α, ε dependent decay law (Fig. 13). Our results show that in the $\varepsilon\to 0$ limit the decay law is compatible with a power law (the exponent seems to be higher than the one of the decay of correlations), while for high values of ε the decay law appears to be at least exponential. As a guess we claim a decay law $n^{-b}f(\varepsilon,n)$, where $f(\varepsilon,n)$ should be bounded by the decay law for translation and identity, Eq. (16). We checked that n_* corresponds to the beginning of the transition from the delta function to the asymptotic error distribution function (not shown) and that Eq. (2) holds for ρ_∞^ε (which is shown in Fig. 14). We believe that the proposed decay law is also satisfied by the annealed random correlation integral given by the left-hand side of Eq. (6): this is a nice theoretical challenge.

Equation (D1) predicts a divergence for the asymptotic distribution ρ_∞^ε in 0 whenever $\alpha>1/2$. We have indeed verified that the height of $\rho_\infty^\varepsilon(0)$, numerically computed using a Monte Carlo sampling with space discretization Δx, grows for the numerically accessible values of Δx, at least as $\log(\Delta x)$.

D. Quadratic map

We consider in this section the quadratic map $T_a x=a-x^2$, $a>0$. The image under T_a of $[-\sqrt{2a},\sqrt{2a}]$ is $[-a,a]$ and thus for $a<2$ we can define the perturbed map $T_{a,\varepsilon\xi}x=a-x^2+\varepsilon\xi$ from $[-\sqrt{2a},\sqrt{2a}]$ to itself provided that $\varepsilon<\sqrt{2a}-a$.

This class of maps has been investigated in Ref. 27 from the point of view of stochastic stability. First of all the authors restricted the choice of the parameter a to the set of positive measure for which there exists a unique absolutely continuous invariant measure with density h (Jakobson's theorem[28]). For those values, the map satisfies also the Benedicks–Carleson[14] conditions which were important for establishing the other perturbative results under the additive noise, namely, (i) the existence of an absolutely continuous stationary measure with density h_ε which converges in the $\mathcal{L}_m^1$ norm to h (stochastic stability) and (ii) the existence of exponential decay of correlations for the unperturbed map and for the perturbed system with decay rates which are uniformly bounded in the noise (provided ε is small enough), as in formulas (5) and (6). The latter (see Ref. 9) allows us to apply Theorem 1 on the fidelity so that the estimate (12) for the rate of convergence to the characteristic function of the asymptotic error holds. We verified, through a bifurcation analysis, that in a neighborhood of $a=1.6$ the map is chaotic, and thus we have used this value for our investigation.

After a transient (which is due to the difference between the uniform distribution we use as initial condition for our Monte Carlo method and the invariant measure of the map) there is a plateau that ends at n_*, whose ε dependence is in qualitative agreement with Eq. (20), Fig. 15. To n_* corresponds the beginning of the transition of the error distribution function (not shown). The asymptotic error distribution is shown in Fig. 16 [we have verified that the same result can also be obtained using Eq. (2)].

E. Standard map

We study the standard map defined as

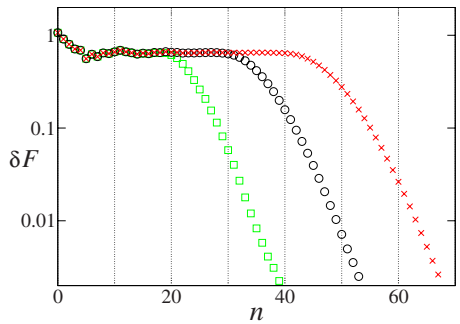

FIG. 15. (Color online) Decay of fidelity for the quadratic map, $a=1.6$, Monte Carlo integration with $N=10^8$. Green squares: $\varepsilon=10^{-4}$. Black circles: $\varepsilon=10^{-6}$. Red crosses: $\varepsilon=10^{-8}$.

$$T\mathbf{x}=\begin{cases} y'=y+K\sin(x) \\ x'=x+y'. \end{cases} \tag{30}$$

We analyze its behavior considering three values of K: $K=10$ (chaotic behavior), $K=10^{-2}$ (regular behavior), and $K=2$ (mixed behavior). We recall that the breakup of the last invariant curve corresponding to the golden mean frequency occurs for $K\simeq 1$.

Case $K=10$: The chaotic case can be easily understood using the framework developed for other maps. For the decay of fidelity we have a plateau, followed by an outset of decay that occurs at n_* in qualitative agreement with Eq. (20) [(a) of Fig. 17]. n_* corresponds to the beginning of the transient of the error function. The asymptotic error function ρ_∞^ε is triangular and Eq. (2) applies.

Case $K=10^{-2}$: In the regular regime there is no clear outset of decay, but just an ε dependent decay law [(b) of Fig. 17]. The asymptotic error function is reached when the fidelity reaches a value of a few orders of magnitude lower than its initial value. The asymptotic error function is triangular and Eq. (2) holds. The decay for y follows the same law as rotations on the circle, while the decay for x is quicker. This can be easily understood by considering the map where $K\sin(x)$ is replaced by $K\xi$, where ξ is a random variable in $[-1,1]$. In the continuum limit $K\to 0$, see Appendix C, we have a diffusive process with Gaussian distribution where the mean square deviation is K^2n for the y variable, K^2n^3 for the x variable proving that the relaxation for the latter is faster.

Case $K=2$: For $K=2$ the system exhibits features of both regular and chaotic maps. The decay of fidelity presents a plateau ending at n_* in agreement with Eq. (20). This phase is followed by a quick, almost ε independent decay phase, and then by a slower ε dependent phase (Fig. 18). After the first quick decay phase we reach an asymptotic error function for the chaotic component only, while if ε is low enough, we still have a δ function for the regular component (Fig. 19). For low values of ε we can consider this as a "metastable error distribution function" since it does not change during a time scale much longer than the decay of the chaotic component. The study of the ε dependent decay phase of the regular component in a map with mixed behavior is more difficult than for a regular map, probably due to the interaction between the chaotic and regular components. Indeed, for purely chaotic and regular maps we found that the decay of fidelity was almost independent of the function ψ, and thus we limited ourselves to the study of the less computationally expensive $\psi(\mathbf{x})=x$. But for the standard map with $K=2$ even when the fidelity for $\psi(\mathbf{x})=x$ has reached a value of a few orders of magnitude lower than its initial value, the error function has not reached its asymptotic value (triangular distribution). Since the error distribution ρ_ε^n is given by the Fourier transform of $\varphi_\varepsilon^n(u)$, i.e., by the fidelity computed using $\psi_1=\psi_2^*=e^{iux}$, the time scales of the transient of ρ_ε^n are determined by the decay of fidelity of e^{iux}. While for all the previously studied systems the decay of fidelity for e^{iux} resulted to be u independent, and thus the system had a single decay time scale, for the standard map with $K=2$ the decay of e^{iux} results to be strongly u dependent (see Fig. 20; the change in slope around $n\approx 50$ corresponds to the end of the decay of the chaotic component and the beginning of the "metastable" phase, which is quite short for $\varepsilon=10^{-1}$ but considerably

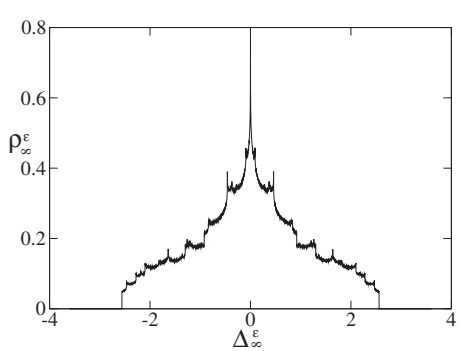

FIG. 16. ρ_∞^ε for the quadratic map, $a=1.6$, $\varepsilon=10^{-8}$. Monte Carlo sampling using $N=10^9$ and $\Delta x=10^{-3}$.

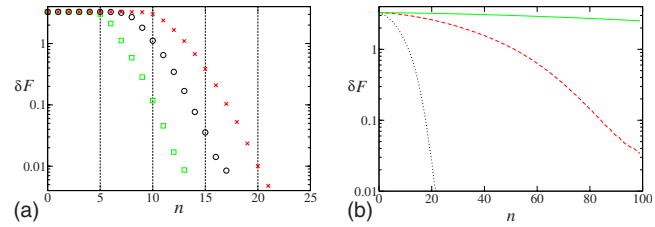

FIG. 17. (Color online) Decay of fidelity for the standard map, x observable, Monte Carlo integration with $N=10^7$. (a) $K=10$ (green squares: $\varepsilon=10^{-4}$; black circles: $\varepsilon=10^{-6}$; red crosses: $\varepsilon=10^{-8}$). (b) $K=10^{-2}$ (black, dotted: $\varepsilon=10^{-1}$; red, dashed: $\varepsilon=10^{-2}$; green: $\varepsilon=10^{-3}$).

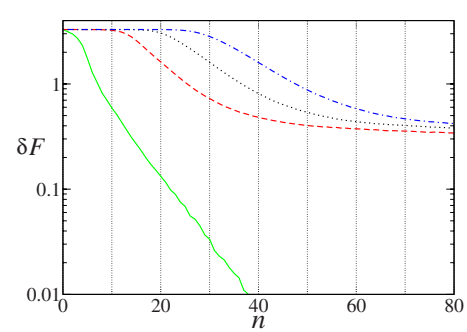

FIG. 18. (Color online) Decay of fidelity for the standard map, x observable, $K=2$, Monte Carlo integration with $N=10^7$. Green: $\varepsilon=10^{-1}$. Red, dashed: $\varepsilon=10^{-4}$. Black, dotted: $\varepsilon=10^{-6}$. Blue, dot-dashed: $\varepsilon=10^{-8}$.

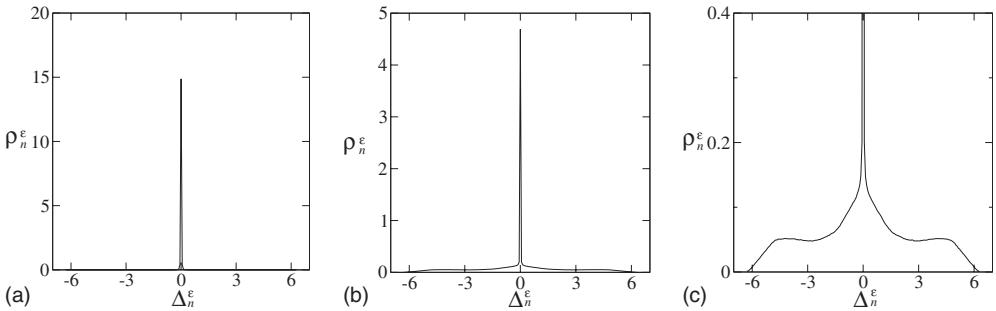

FIG. 19. ρ_n^ε for the standard map, $K=2$, $\varepsilon=10^{-4}$, x observable. (a) $n=9$; (b) $n=49$; (c) detail of the metastable distribution (ρ_{49}). Monte Carlo sampling using $N=10^7$ and $\Delta x=\pi/50$.

longer for lower values of ε), and thus the regular component of a map with mixed behavior has not a single decay scale. We have verified that when the fidelity computed using e^{ix}, which, on the basis of our numerical tests, has probably the longest decay time, reaches a value of $\approx 10^{-3}$, we have the convergence to the triangular asymptotic error distribution ρ_∞^ε.

V. CONCLUSIONS

We have analyzed the statistical properties of the error introduced by an additive random noise in a discrete dynamical system by comparing the distributions obtained from Monte Carlo computations and from the fidelity, which, for a suitable choice of the observables, provides the Fourier transform of the pdf of the error. This pdf is obtained in the limit of large iteration time and the rate of this convergence is very important to discriminate between regular and chaotic motions. For rotations and Bernoulli maps an exact result and an optimal estimate for the convergence rate are obtained. The exponential convergence rate for regular maps and the superexponential one for chaotic maps appear to be quite general as we indicate by several numerical examples. The initial distribution of errors is a Dirac δ function with support at zero, whereas the asymptotic distribution depends on the invariant and the stationary measures. When both are Lebesgue the asymptotic distribution is triangular as for two points randomly chosen on an interval. For measures absolutely continuous with respect to Lebesgue the asymptotic distribution is smooth, whereas it is spiky for singular continuous measures typical of attractors with a Cantorian structure (fractals). As we said above, the ergodic properties of the map are reflected in the way the asymptotic limit is reached: the exponential and superexponential convergence rates are the same as for a random walk when the deterministic evolution is linear or exponential as it can be easily proved in the continuum limit. Whereas the asymptotic limit is reached smoothly for regular maps, for the chaotic ones there is a sharp transition whose location depends only on the perturbation strength. For maps with chaotic and regular invariant regions, such as the standard map short after the breakup of the last invariant curve, there is first a sharp transition followed by a smooth decay. Finally the procedure we outlined applies to the analysis of roundoff errors for the numerical maps, a key issue in the numerical analysis of dynamical systems. We have already applied the procedure developed in this paper to analyze the roundoff errors and the results will be soon submitted for publication. We can anticipate that the global error grows linearly for regular maps and exponentially for chaotic maps, while the asymptotic error distribution reflects the properties of the invariant measure. The convergence rate of fidelity can be quite different from the one observed for additive noise due to the deterministic nature of roundoff, nevertheless by increasing the complexity of the map the "pseudorandom" character of roundoff errors becomes more pronounced, and the decay law becomes, in particular for chaotic maps, equivalent to that of maps perturbed with additive noise. To conclude we claim that we have provided a reliable and constructive tool to investigate analytically and numerically the perturbations induced by random errors. This procedure can be applied also to numerical roundoff errors even though in that case no rigorous general results can be formulated because the algorithms implemented in finite precision arithmetic are hardware dependent.

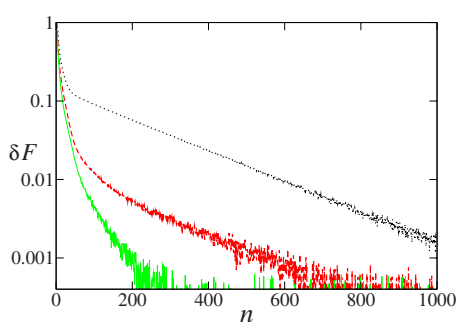

FIG. 20. (Color online) Decay of fidelity for the standard map, $K=2$, $\varepsilon=10^{-1}$, Monte Carlo integration with $N=10^7$. Black, dotted: $\psi_1=\psi_2^*=e^{ix}$. Red, dashed: $\psi_1=\psi_2^*=e^{i2x}$. Green: $\psi_1=\psi_2^*=e^{i3x}$.

ACKNOWLEDGMENTS

F.Z. has been partially supported by the GDRE 224 GREFI-MEFI (jointly sponsored by the French CNRS and the Italian INDAM). The authors thank the anonymous referees whose remarks and suggestions contributed to improve the paper.

APPENDIX A: COMPARISON TO SOME RESULTS BY SAUER

We now compare our results with the work of Sauer in Ref. 13. He considered a smooth observable g on the phase space X and the algebraic difference

$$\Delta(g) \equiv \langle g\rangle_{\text{computed}} - \langle g\rangle_{\text{true}},$$

where $\langle g\rangle_{\text{true}}$ is the ergodic average computed along the true trajectory of T and $\langle g\rangle_{\text{computed}}$ is the ergodic average computed along the perturbed orbit with noise size ε. Sauer proposed the following heuristic scaling:

$$\Delta(g) = K\varepsilon^h,$$

where K is a constant and h is an "exponent expressing the severity of the fluctuations of the Lyapunov exponent."[13]

For a map belonging to the class $\mathcal{M}$, we simply have $\langle g\rangle_{\text{true}} = \int_X g d\mu$. The ergodic average for the random perturbations introduced in Sec. II C will be

$$\lim_{n\to\infty}\frac{1}{n}\sum_{l=0}^{n-1} g(T_{\omega_l}T_{\omega_{l-1}}\cdots T_{\omega_0}x).$$

For the maps in $\mathcal{M}$ the stationary measure is ergodic and this means that the previous Birkhoff sum goes to $\int_X g d\mu_\varepsilon$, for x chosen m—almost everywhere and for almost all the realizations $\boldsymbol{\omega}$ taken with respect to the measure $\theta_\varepsilon^{\mathbb{N}}$; see, for instance, Ref. 29. It is therefore reasonable to put $\langle g\rangle_{\text{computed}} = \int_X g d\mu_\varepsilon$ in such a way that

$$\Delta(g) = \int_X g d\mu_\varepsilon - \int_X g d\mu$$

[compare with (i) in Remark 2]. Now, let us suppose that the map $T \in \mathcal{M}$ has an invariant measure μ which is absolutely continuous with respect to the Lebesgue measure m with density h; we suppose also that the stationary measure μ_ε is absolutely continuous with density h_ε. The systems in $\mathcal{M}$ usually enjoy the *strong* stochastic stability property which means the convergence of h_ε to h in the $\mathcal{L}_m^1$ norm. The paper[24] quotes several examples where this $\mathcal{L}_m^1$ convergence is explicitly computed for additive noise, with rigorous arguments or numerically (even for systems outside $\mathcal{M}$), as a function of the noise size ε; the scalings found are of the type

$$\|h - h_\varepsilon\|_{\mathcal{L}_m^1} \le \text{const}\ \ \varepsilon^\gamma, \tag{A1}$$

where γ is an exponent depending upon the map T. This exponent seems related to the smoothness of the map rather than to the Lyapunov exponent. For example, for continuous uniformly expanding maps of the circle $\gamma=2$, while $\gamma=1$ if the map has discontinuities and it is therefore piecewise expanding. For Misiurewicz quadratic maps (see also Sec. IV D), $\gamma=0.5$ and it ranges between 0.3 and 0.7 for the intermittent map investigated in Sect. IV C. We have also seen that there are examples for which the invariant and the stationary measure are the same, $h=h_\varepsilon$, but the pdf of the asymptotic error for the observable identity $f(x)=x$ is a smooth function whose support has diameter twice the support of the invariant measure.

Since, by Hölder inequality,

$$|\Delta(g)| \le \|g\|_{C^0}\|h - h_\varepsilon\|_{\mathcal{L}_m^1}\|g\|_{C^0}\text{const}\ \ \varepsilon^\gamma,$$

the comparison with the previous bound claimed by Sauer is not obvious especially for the meaning of the scaling exponent of ε. One possible explanation, which deserves better investigation, is that the fluctuations of the Lyapunov exponent play a role whenever we replace $\langle g\rangle_{\text{computed}}$ with the Birkhoff sum $1/n\Sigma_{l=0}^{n-1} g(T_{\omega_l}T_{\omega_{l-1}}\cdots T_{\omega_0}(x))$ for finite n and we take into account the limits for small ε and large n.

Another explanation is that Sauer's result holds for diffeomorphisms admitting a SRB measure which is singular with respect to Lebesgue and with more than one Lyapunov exponent. In this case we lose the comparison of the densities given by Eq. (A1) and we should evaluate directly the difference $\int_X g d\mu_\varepsilon - \int_X g d\mu$: this is done, for example, for uniformly hyperbolic attractors in Ref. 30 and for the Hénon attractor in Ref. 15, but there is no explicit scaling in ε.

APPENDIX B: COMPUTATION OF FIDELITY FOR *qx* mod 1

The iterated perturbed map is defined as

$$T_\varepsilon^n = q^n x + \varepsilon(q^{n-1}\xi_1 + q^{n-2}\xi_2 + \cdots + q\xi_{n-1} + \xi_n)\text{mod } 1.$$

The fidelity for functions ϕ, ψ which are piecewise C^1 with a finite number of discontinuities is given by

$$F_n^\varepsilon = \sum_{k,k'} \phi_k\psi_{k'}\int_0^1 e^{2\pi i q^n(k-k')x}dx\int_{-1}^1 \frac{d\boldsymbol{\xi}}{2^n}e^{2\pi i k'\varepsilon(q^{n-1}\xi_1+\cdots+\xi_n)}$$
$$= \phi_0\psi_0 + \sum_{|k|\ge 1}\phi_k\psi_{-k}S_{n,q}(k\varepsilon). \tag{B1}$$

It is trivial to check that the decay of fidelity for any translation on the torus is equivalent to that of the identity $Tx=x$, and thus since $S_{n,q}(x)\equiv S^n(x)$, Eq. (B1) implies both Eqs. (14) and (17).

To estimate $S_{n,q}(x)$ we can use the bound (15) for $S(x)$, but we have to distinguish between three regions (we assume $x>0$, in the general case substitute x with $|x|$): region 1, where $q^{n-1}x<1$, in which we can use, setting $\alpha=\log(2\pi)$

$$|S_{n,q}(x)| \le e^{-\alpha x^2(1+q^2+\cdots q^{2(n-1)})} \le e^{-\alpha x^2 q^{2(n-1)}},$$

region 3 where

$$xqx\cdots q^{n-1}x = x^n q^{1+2+\cdots+n-1} = (xq^{(n-1)/2})^n > 1$$

or, equivalently, $xq^{(n-1)/2}>1$, and thus we can use

$$|S_{n,q}(x)| \le (2\pi x q^{(n-1)/2})^{-n},$$

and an intermediate region 2 where $xq^{-(n-1)/2}<1<xq^n$. To analyze the behavior of the function in the latter region let us assume that $xq^{m-1}<1<xq^m$ with integer $(n-1)/2<m<n$. We can estimate in a different way the terms with xq^l greater or smaller than 1, and thus

$$|S_{n,q}(x)| \le \frac{(2\pi)^{-(n-m)}}{xq^m xq^{m-1}\cdots xq^{n-1}} e^{-\alpha x^2(1+q^2+\cdots q^{2(m-1)})}$$
$$\le (2\pi x q^{(n+m-1)/2})^{-(n-m)} e^{-\alpha x^2 q^{2(m-1)}}$$
$$\le (2\pi q^{(n-m-1)/2})^{-(n-m)} e^{-\alpha x^2 q^{2(m-1)}}.$$

We can thus use the following bound for $S_{n,q}(x)$:

$$|S_{n,q}(x)| \le \begin{cases} \exp(-\alpha x^2 q^{2(n-1)}) & \text{if } xq^{n-1} < 1 \\ (2\pi q^{(n-m-1)/2})^{-(n-m)} e^{-\alpha x^2 q^{2(m-1)}} & \text{if } xq^{m-1} < 1 < xq^m \text{ with } (n-1)/2 < m < n \\ (2\pi x q^{(n-1)/2})^{-n} & \text{if } xq^{(n-1)/2} > 1, \end{cases}$$

where we have once again $\alpha = \log(2\pi)$. [When $q=1$ there is no region 2, and in region 1 the more accurate bound $S^n(x) \le e^{-\alpha x^2 n}$ can be used.]

Using the estimates on $S_{n,q}(x)$ we provide bounds to the fidelity in three different regions. It is convenient to introduce an integer n_* defined by $n_* = \{-\log_q \varepsilon\}$, where $\{x\}$ denotes the integer closest to the real x, so that

$$\varepsilon \simeq q^{-n_*}.$$

- Region I: $\varepsilon q^{n-1} < 1$. Using the Fourier expansion for the fidelity (B1) we write

$$|F_n - \phi_0\psi_0| \le \sum_{k\neq 0} |\phi_k \psi_{-k}||S_{n,q}(k\varepsilon)| = R_1 + R_2 + R_3,$$

where the term R_1 corresponds to the contribution of all the Fourier components with $|k|\varepsilon q^{n-1} < 1$, the term R_2 to the components with $|k|\varepsilon q^{(n-1)/2} < 1 < |k|\varepsilon q^{n-1}$, and the term R_3 to the components with $|k|\varepsilon q^{(n-1)/2} > 1$.

The following bound holds for the first term R_1,

$$R_1 \le \sum_{|k|=1}^{(\varepsilon q^{n-1})^{-1}} |\phi_k \psi_{-k}| e^{-\alpha\varepsilon^2 k^2 q^{2(n-1)}}$$
$$\le e^{-\alpha\varepsilon^2 q^{2(n-1)}} 2 \sum_{k=1}^{(\varepsilon q^{n-1})^{-1}} \frac{1}{k^2} \le 2(2-\varepsilon q^{n-1}) e^{-\alpha\varepsilon^2 q^{2(n-1)}},$$

where we have assumed once again that the Fourier coefficients decay as $|k|^{-1}$ and we have used the following estimate:

$$\sum_{k=A}^{B} \frac{1}{k^2} \le \frac{1}{A^2} + \int_A^B \frac{dk}{k^2} = \frac{1}{A^2} + \frac{1}{A} - \frac{1}{B} \le \frac{2}{A} - \frac{1}{B}$$

for $B > A \ge 1$. The second term R_2 has the following bound:

$$R_2 \le \sum_{m=(n+1)/2}^{n-1} (2\pi q^{(n-m-1)/2})^{-(n-m)} \sum_{|k|=(\varepsilon q^m)^{-1}}^{|k|=(\varepsilon q^{m-1})^{-1}} \frac{e^{-\alpha k^2 \varepsilon^2 q^{2(m-1)}}}{k^2}$$
$$\le \sum_{m=(n+1)/2}^{n-1} (2\pi q^{(n-m-1)/2})^{-(n-m)} e^{-\alpha/q^2} 2\varepsilon q^m (2-q^{-1})$$
$$\le \frac{e^{-\alpha/q^2}}{2\pi} 2\varepsilon \left(2 - \frac{1}{q}\right) \sum_{m=n+1/2}^{n-1} q^m$$
$$\le 4\varepsilon q^n \frac{e^{-\alpha/q^2}}{2\pi(q-1)} \le 2\varepsilon q^{n-1}.$$

For the third term R_3 we have the bound

$$R_3 \le \sum_{|k|\ge(\varepsilon q^{(n-1)/2})^{-1}}^{\infty} \frac{1}{k^2} \frac{1}{(2\pi\varepsilon|k|q^{(n-1)/2})^n}$$
$$\le \frac{2}{(2\pi\varepsilon q^{(n-1)/2})^n} \left((\varepsilon q^{(n-1)/2})^{n+2} + \int_{(\varepsilon q^{(n-1)/2})^{-1}}^{\infty} \frac{dk}{k^{n+2}} \right)$$
$$= \frac{2}{(2\pi)^n} \varepsilon q^{(n-1)/2} \left(\frac{1}{n+1} + \varepsilon q^{(n-1)/2} \right)$$
$$\le \frac{4}{(2\pi)^n} \varepsilon q^{(n-1)/2}.$$

Finally the estimate in this region reads

$$|F_n - \phi_0\psi_0| \le 2(2-\varepsilon q^{n-1}) e^{-\alpha\varepsilon^2 q^{2(n-1)}} + 2\varepsilon q^{n-1} + \frac{4}{(2\pi)^n} \varepsilon q^{(n-1)/2}, \tag{B2}$$

which for $q=1$ leads to Eq. (16).

- Region II: $\varepsilon q^{(n-1)/2} < 1 < \varepsilon q^{n-1}$. In this region the estimate is not very accurate. First of all R_1 vanishes since the upper limit in the sum, namely, $(\varepsilon q^{n-1})^{-1}$, is smaller than the lower limit. The second term R_2, which is evaluated above for $\varepsilon q^{n-1} \simeq 1$, is of order 1, whereas the last term R_3 is small with respect to 1.
- Region III: $\varepsilon q^{(n-1)/2} > 1$. In this region the contributions of R_1 and R_2 vanish and we are left just with R_3 which reads

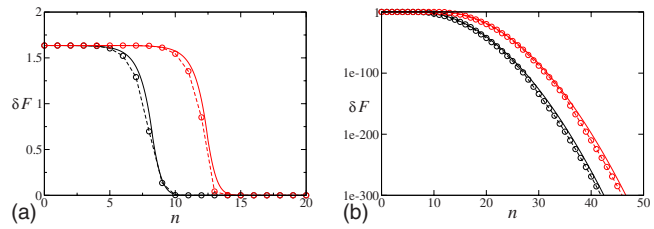

FIG. 21. (Color online) Comparison between the analytical result (B1) (dashed lines and circles) and the estimate (B5) (continuous lines) using $\phi_k=\psi_k=k^{-1}$ truncated at $k=100$. Black: $\varepsilon=10^{-4}$. Red (gray in black and white): $\varepsilon=10^{-6}$ [(b) logarithmic plot].

$$R_3 \le \sum_{|k|=1}^{\infty} \frac{1}{k^2} \frac{1}{(2\pi\varepsilon|k|q^{(n-1)/2})^n}$$
$$= 2\left(1+\int_1^{\infty} \frac{dk}{k^{n+2}}\right) \frac{1}{(2\pi\varepsilon q^{(n-1)/2})^n}$$
$$= \frac{n+2}{n+1} \frac{2}{(2\pi\varepsilon q^{(n-1)/2})^n}. \tag{B3}$$

1. Fit and comparison to Monte Carlo simulations

The validity of the previous estimates has been checked with numerical calculations. We first write Eq. (B3) using $\varepsilon=q^{-n_*}$ so that

$$R_3 \le 3\left(\frac{q^{1/2}}{2\pi}\right)^n q^{nn_*} q^{-n^2/2} = 3q^{n_*^2/2}\left(\frac{q^{1/2}}{2\pi}\right)^n q^{-(n-n_*)^2/2},$$

valid for $\varepsilon q^{(n-1)/2}>1$. From the estimate (B2) and the present one we finally obtain

$$|F_n-\phi_0\psi_0| \le \begin{cases} 2(2-\varepsilon q^{n-1})e^{-\alpha\varepsilon^2 q^{2(n-1)}} + 2\varepsilon q^{n-1} \\ \quad \text{if } n<n_*+1 \\ 3q^{n_*^2/2}\left(\dfrac{q^{1/2}}{2\pi}\right)^n q^{-(n-n_*)^2/2} \\ \quad \text{if } n \ge 2n_*+1. \end{cases} \tag{B4}$$

We can fit the fidelity with a formula derived from the previous estimates by extending the estimate in region III to region II according to

$$|F_n-\phi_0\psi_0| \simeq \begin{cases} Ae^{-\alpha q^{2(n-n_*)}} & \text{if } n \le n_* \\ Ae^{-\alpha'} q^{-(n-n_*)^2/2} & \text{if } n > n_*, \end{cases} \tag{B5}$$

where A is a constant of order 1. We can evaluate the width of the transition Δn requiring that at $n=n_*-\Delta n$ the decay of fidelity $\delta F_n=|F_n-\phi_0\psi_0|$ assumes a value some percent below A [at $n=n_*$ its value is $Ae^{-\alpha}=A(2\pi)^{-1}=0.16A$]. Choosing, for instance, $\delta F_{n_*-\Delta n}=Ae^{\alpha e^{-4}}\simeq 0.97A$ we find

$$\Delta n = \frac{2}{\log q}.$$

The validity of the analytical result (B1) has been checked with a Monte Carlo simulation (Fig. 1). We found (Fig. 21) that the analytical result (B1) can be fitted very well by Eq. (B5).

We outline that due to the extremely quick decay of the $e^{-\alpha\varepsilon^2 q^{2(n-1)}}$ term around n_*, the fit (B5) can be sketched as a plateau of length $n_*(\varepsilon)$ followed by an ε independent decay law.

APPENDIX C: THE CONTINUUM LIMIT

A map on the torus $\mathbb{T}$ with a random perturbation

$$x_{n+1} = x_n + \Delta t\phi(x_n) + \varepsilon\sqrt{\delta t}\xi_n,$$

where ξ_n are random variables with zero average and unit variance, becomes in the limit $\Delta t \to 0$ the Langevin equation

$$\dot{x} = \phi(x) + \varepsilon\xi(t),$$

setting $\xi(t)dt=dw(t)$ where $w(t)$ is a Wiener process and $\xi(t)$ a distribution known as white noise. The probability density distribution $\rho(x,t)$ satisfies the Fokker–Planck equation

$$\frac{\partial\rho}{\partial t} + \phi(x)\rho = \frac{\varepsilon^2}{2}\frac{\partial^2\rho}{\partial x^2}$$

with boundary conditions $\rho(0,t)=\rho(1,t)$ and initial condition $\rho(x,0)=\rho_0(x)$. The fundamental solution $G(x,t;x_0,0)$ satisfies the same equation with initial condition $G(x,0;x_0,0)=\delta(x-x_0)$. As a consequence, we have

$$\rho(x,t) = \int_0^1 dx_0 G(x,t;x_0,0)\rho_0(x_0).$$

Letting $G_{\mathbb{R}}$ be the fundamental solution defined in $\mathbb{R}$ the corresponding solution for the torus $\mathbb{T}$ is given by

$$G_\epsilon(x,t;x_0,t) = \sum_{n=-\infty}^{+\infty} G_{\mathbb{R}}(x+n,t;x_0,0) = \sum_{k=-\infty}^{+\infty} C_k(t)e^{2\pi ikx}.$$

Simple calculations show that for $\phi(x)=\Omega$ and $\phi(x)=Ax$ the Fourier coefficients are given by

$$C_k(t) = e^{-2\pi ik(x_0+\Omega t)}e^{-2\pi^2k^2\epsilon^2 t} \quad \text{if } \phi=\Omega,$$

$$C_k(t) = e^{-2\pi ikx_0e^{At}}e^{-2\pi^2k^2\epsilon^2(e^{2At}-1)/2A} \quad \text{if } \phi=Ax.$$

We notice that the unperturbed $\epsilon=0$ fundamental solution is $G_0(x,t;x_0,t)=\delta(x-S_t(x_0))$, where $S_t(x_0)=x_0+\Omega t$ if $\phi=\Omega$ and $S_t(x_0)=x_0e^{At}$ if $\phi=Ax$.

Given two smooth observables $f(x)$, $g(x)$ the correlations and the fidelity are defined by

$$C(t) = \int_0^1 dx_0 f(x_0)\int_0^1 dx G(x,t;x_0,0)g(x),$$

$$F(t) = \int_0^1 dx_0 f(S_t(x_0))\int_0^1 dx G(x,t;x_0,0)g(x).$$

After the Fourier expansion of f and g and denoting with

$$F(t)=\sum_{k=-\infty}^{+\infty}\sum_{k'=-\infty}^{+\infty} f_{-k}e^{-2\pi^2k'^2\sigma^2(t)}g_{k'}\int_0^1 dx_0 e^{-2\pi i S_t(x_0)(k-k')},$$

the mean square deviation of the stochastic processes satisfying $\dot{\eta}=\Omega+\epsilon\xi$ is $\sigma^2(t)=\epsilon^2 t$, whereas for $\dot{\eta}=Ax+\epsilon\xi$ it is given by $\sigma^2(t)=\epsilon^2(e^{2At}-1)/2A$. The last integral is $\delta_{k',k}$ if $S_t(x_0)=x_0+\Omega t$ and $e^{i\theta}\theta^{-1}\sin\theta$ with $\theta=\pi e^{At}(k'-k)$, which approaches $\delta_{k',k}$ as $t>0$ grows. As a consequence we may compare the results with the translations on the torus and the map $qx \bmod 1$ by setting $\omega=\Omega\Delta t$, $q=1+A\Delta t$, and $\epsilon_{\text{map}}=\epsilon\sqrt{\Delta t}$. Agreement is found with the fidelity for the maps if we let $\Delta t\to 0$ and $n\to\infty$ so that $n\Delta t=t$ finite.

APPENDIX D: LÉVY'S INVERSION FORMULA

Let us consider a 1D map on the unit interval [0,1] and the observable identity $f(x)=x$. Suppose, moreover, that μ and μ_ε have absolutely continuous invariant densities h and h_ε, respectively, which are $\mathcal{L}_m^1$ very close in such a way that $\varphi_\infty^\varepsilon$ is approximately given by $\varphi_\infty^\varepsilon(u)=|\int_{[0,1]}e^{iux}h(x)dx|^2$. Standard results on Fourier series immediately imply that $\varphi_\infty^\varepsilon$ is uniformly continuous on $\mathbb{R}$, bounded and vanishing at infinity (Riemann–Lebesgue). We now consider the interesting cases given by the intermittent maps of Sec. IV C and the quadratic maps of Sec. IV D for which the invariant density behaves like $h(x)\sim x^{-\alpha}$, with $0<\alpha<1$ for the intermittent maps and $\alpha=0.5$ for the particular quadratic map with $a=2$, and whenever x is close to 0 (for the quadratic map a change in variable brings the singularity from ± 1 to zero). We have, therefore, to investigate the asymptotic behavior for large $|u|$ of the integral

$$\varphi_\infty^\varepsilon(u)=\left|\int_{[0,1]}\frac{e^{iux}r(x)}{x^\alpha}dx\right|^2,\quad 0<\alpha<1,$$

where r is a bounded smooth function in the interval [0,1]. Now we have (Ref. 31, p. 519)

$$\left|\int_{[0,1]}\frac{e^{iux}r(x)}{x^\alpha}dx\right|=\mathcal{O}(|u|^{\alpha-1}),\quad |u|\ \text{large}. \tag{D1}$$

We could therefore conclude that whenever $\alpha<1/2$ the characteristic function $\varphi_\infty^\varepsilon$ is summable and we can apply the Lévy inversion formula to get the density of the distribution function of the asymptotic error. Instead when $1/2\le\alpha<1$ we should use a generalization of Eq. (11); if we call Φ_∞^ε the distribution function of $\Delta_\infty^\varepsilon$ and if $-\infty<a<b<\infty$ are continuity points for Φ_∞^ε, then (Ref. 12, p. 264)

$$\Phi_\infty^\varepsilon(b)-\Phi_\infty^\varepsilon(a)=\lim_{C\to\infty}\frac{1}{2\pi}\int_{-C}^{C}\frac{e^{-ita}-e^{-itb}}{it}\varphi_\infty^\varepsilon(t)dt.$$

The integral on the right-hand side of the preceding formula is of course convergent for $0<\alpha<1$ and whenever $|C|$ goes to infinity. We have nevertheless proceeded to the numerical computation of the improper integral $\rho_\infty^\varepsilon(t)=(2\pi)^{-1}\int_{-\infty}^{\infty}e^{-iut}\varphi_\infty^\varepsilon(u)du\sim(2\pi)^{-1}\int_{-\infty}^{\infty}e^{-iut}/(u^{2-2\alpha})du$, where $2-2\alpha\le 1$ for $1/2\le\alpha$. We choose for simplicity $2-2\alpha<1$, since the integrand $u^{2\alpha-2}$ is the asymptotic approximation, for large $|u|$, of the characteristic function $\varphi_\infty^\varepsilon(u)$, and this one is surely integrable in the neighborhood of zero. It is well known that the Fourier transform of $u^{2\alpha-2}$ and for $2-2\alpha<1$ is of order $t^{1-2\alpha}$ in the *distribution* sense.[32] Therefore the density $\rho_\infty^\varepsilon(t)$ computed numerically blows up to infinity for t close to zero and we observed this fact for the intermittent and the quadratic map described above. We believe the same happens for the singular measure of the Baker map, but we do not even have a heuristic handling for this.

[1] D. Knuth, *The Art of Computer Programming* (Addison-Wesley, Reading, 1969), Vol. 2.
[2] A. Katok and B. Hasselblatt, *Introduction to the Modern Theory of Dynamical Systems* (Cambridge University Press, Cambridge, 1995).
[3] S. M. Hammel, J. A. Yorke, and C. Grebogi, J. Complex. **3**, 136 (1987).
[4] S. M. Hammel, J. A. Yorke, and C. Grebogi, Bull. Am. Math. Soc. **19**, 465 (1988).
[5] C. Grebogi, S. Hammel, J. Yorke, and T. Sauer, Phys. Rev. Lett. **65**, 1527 (1990).
[6] S. N. Chow and K. Palmer, J. Dyn. Differ. Equ. **3**, 361 (1991).
[7] E. S. Van Vleck, SIAM J. Sci. Comput. (USA) **16**, 1177 (1995).
[8] T. Sauer, C. Grebogi, and J. Yorke, Phys. Rev. Lett. **79**, 59 (1997).
[9] C. Liverani, Ph. Marie, and S. Vaienti, J. Stat. Phys. **128**, 1079 (2007).
[10] G. Benenti, G. Casati, and G. Velbe, Phys. Rev. E **67**, 055202 (2003).
[11] H. Hu, Ph. Marie, and S. Vaienti (unpublished).
[12] Y. S. Chow and H. Teicher, *Probability Theory* (Springer-Verlag, Berlin, 1978).
[13] T. Sauer, Phys. Rev. E **65**, 036220 (2002).
[14] M. Benedicks and L. Carleson, Ann. Math. **133**, 73 (1991).
[15] M. Benedicks and M. Viana, Ann. Inst. Henri Poincare, Anal. Non Lineaire **23**, 713 (2006).
[16] D. Bessis, G. Paladin, G. Turchetti, and S. Vaienti, J. Stat. Phys. **51**, 109 (1988).
[17] A. Zygmund, *Trigonometrical Series*, 2nd ed. (Cambridge University Press, Cambridge, 1968).
[18] D. Bessis, J. D. Fournier, G. Servizi, and G. Turchetti, Phys. Rev. A **36**, 920 (1987).
[19] C. Liverani, B. Saussol, and S. Vaienti, Ergod. Theory Dyn. Syst. **19**, 671 (1999).
[20] L. S. Young, Isr. J. Math. **110**, 153 (1999).
[21] H. Hu, Ergod. Theory Dyn. Syst. **24**, 495 (2004).
[22] O. Sarig, Invent. Math. **150**, 629 (2002).
[23] S. Gouëzel, Isr. J. Math. **139**, 29 (2004).
[24] K. K. Lin, Nonlinearity **18**, 659 (2005).
[25] V. Araújo and A. Tahzibi, Nonlinearity **18**, 939 (2005).
[26] M. Blank, Discrete Contin. Dyn. Syst. **21**, 749 (2008).
[27] V. Baladi and M. Viana, Ann. Sci. Ec. Normale Super. **29**, 483 (1996).
[28] M. Jakobson, Commun. Math. Phys. **81**, 39 (1981).
[29] J. Alves and V. Araujo, Asterisque **286**, 25 (2003).
[30] M. Viana, Brazilian Mathematics Colloquium 1997, IMPA.
[31] E. W. Hobson, *The Theory of Functions of a Real Variable* (Dover, New York, 1927), Vol. 2.
[32] R. Strichartz, *A Guide to Distribution Theory and Fourier Transform* (World Scientific, Singapore, 2003).

AUTHOR QUERIES — 026904CHA

#1 Author, because of the number of changes to your article, please check your corrections carefully and send us an email with your approval or any minor corrections you mays till have. Thank you.